

# AM Module training course

AM Module, Day 2  
23-24 April'2025



# Schedule for training course

## Day 2

09:00	Discussion: Home assignment
09:10	Theoretical background: Keyhole, fluid flow and absorptivity model
10:00	Printability maps with example
10:30	Q & A (short break)
10:45	Advanced setup: AM → DICTRA and AM → CET models, Calibration of heat source
11:45	Q & A
12:00	Closing of course

# Discussion: Home assignment

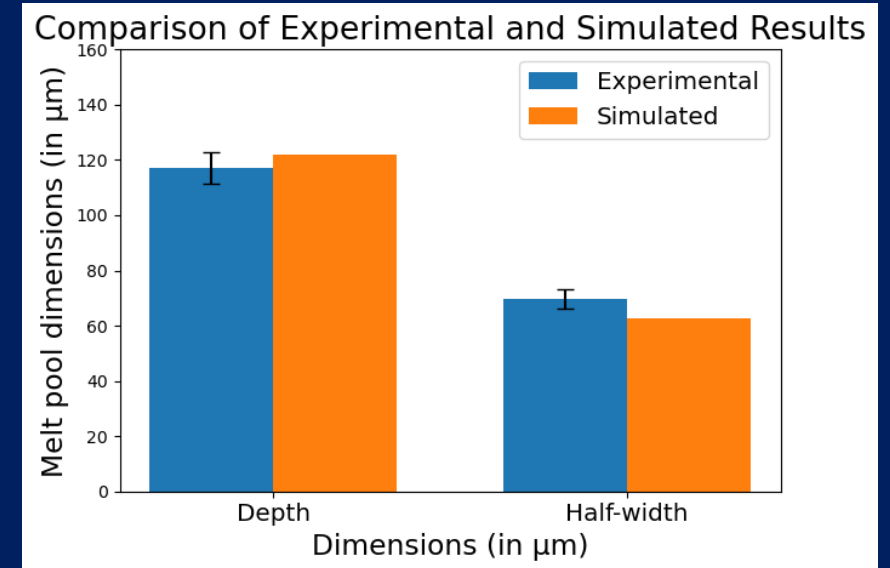
Steady state calculation of a melt pool in 316L stainless steel

Laser power (W)	Speed (mm/s)	Layer thickness ( $\mu\text{m}$ )
215	1000	40

- Gaussian beam with 40  $\mu\text{m}$  radius
  - Consider both with/without keyhole model
- Compare with experimental data and discuss.

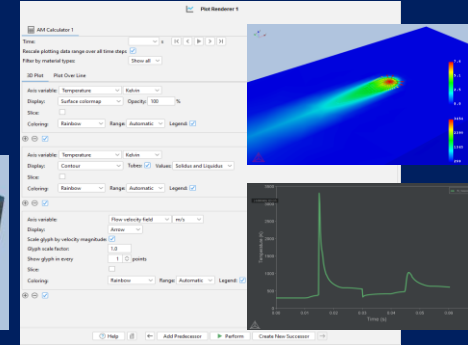
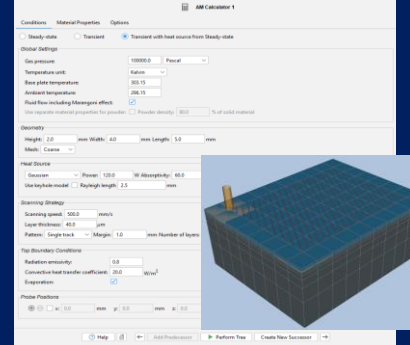
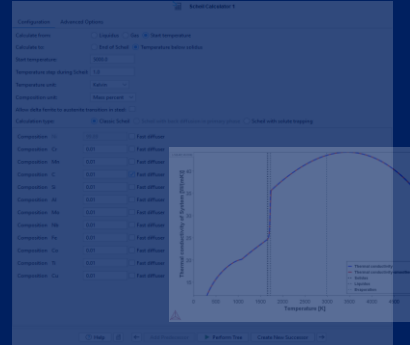
Experimental depth ( $\mu\text{m}$ )	Experimental half width ( $\mu\text{m}$ )
$117.09 \pm 5.8$	$69.6 \pm 3.5$

Simulated depth ( $\mu\text{m}$ )	Simulated half width ( $\mu\text{m}$ )
122	62.7



Tested on 316L stainless steel with keyhole model, gaussian beam in Thermo-Calc 2025a

# Unified Treatment of Material Properties and Process Parameters



Precipitation



Diffusion

System Definer

Extended Scheil  
Calculation

AM Module

Post processing

Export results

Define alloy system, retrieve Thermodynamic and Thermophysical data

Extraction of materials properties from evaporation down to RT including solidification segregation.

Obtain enthalpy, heat capacity, density, thermal conductivity, viscosity, surface tension, volume, molar mass of Gas and driving force for evaporation

Simulate AM with parameters such as: Laser power, Scanning speed and Strategy Layer thickness, Base plate temperature.

Takes into account: Thermal conduction and Fluid flow, Powder density, and heat losses due to radiation and convection and evaporation

Visualize in 3D, over a selected line or at a chosen point over time.

Plottable quantities: Temperature, Flow velocity, Surface tension, Thermal conductivity, Dynamic viscosity and Melt Pool dimension.

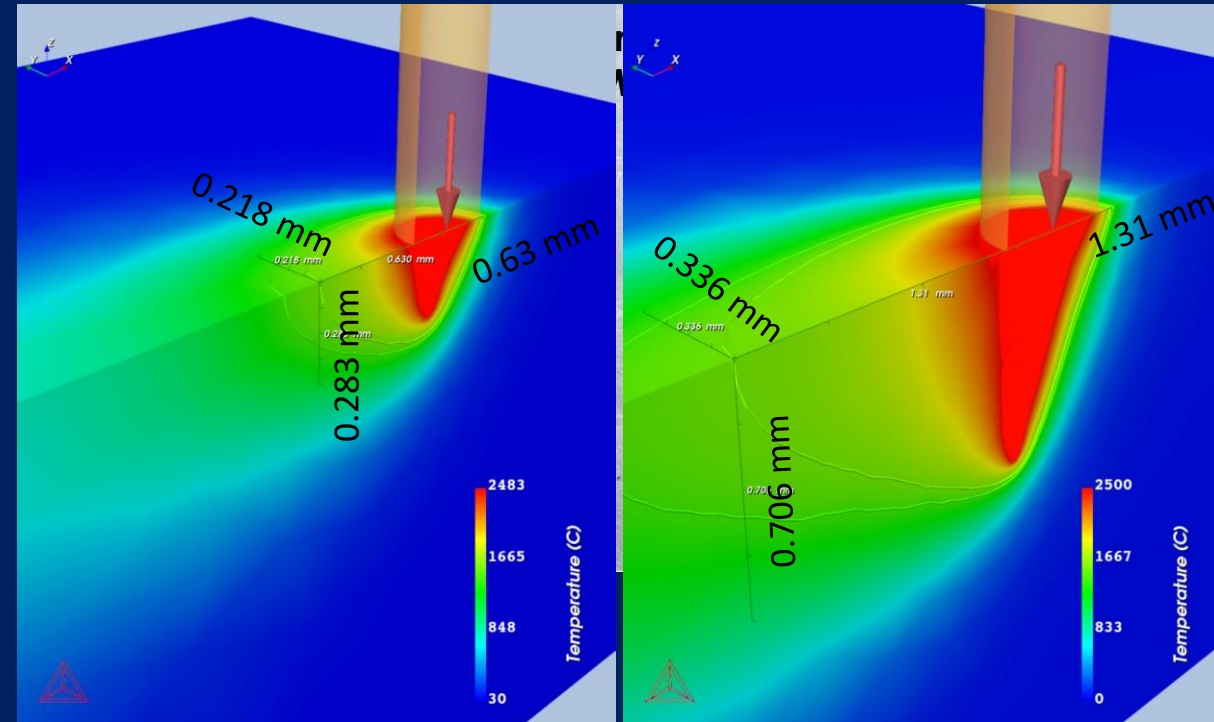
Export time-temperature profile, melt pool dimension and/or temperature distribution in space to other Thermo-Calc modules like DICTRA or PRISMA, or to other external computational softwares.

# Theoretical background

- Keyhole model
- Fluid flow model
- Absorptivity

# Keyhole model

- Keyhole formation is typical when process is run under high power density. This leads to evaporation of the liquid metal
- Evaporation causes transfer of momentum from the metal to the vapour. Conservation of total momentum leads to recoil pressure that pushes down the liquid/ gas interface to form a cavity, known as keyhole
- Since it is computationally expensive to calculate the free surface of keyhole, we use an analytical model (Kaplan, 1994) to pre-compute the keyhole shape and corresponding mesh (hexahedral → tetragonal)
- An example is shown for a  $\beta$  Ti-Al alloy where a normal melt pool at 100W laser power is computed whereas the melt pool reaches keyhole mode at 250W laser power. Based on paper by Laber et al., 2014



100W, 50 mm/s for  $\beta$  Ti-Al alloy

250W, 50 mm/s for  $\beta$  Ti-Al alloy

# Keyhole model

Kaplan model (1994)

High intensity of the beam enabled deep penetration into the workpiece with no appreciable enlargement of the width.

Can solve for keyhole profile at higher welding speeds. Need to solve the front wall and back wall only. Heat loss analytical equations are:

$$\text{Front wall} \left\{ \begin{aligned} q_v(x_f) &= (T_v - T_a)\lambda_{th}Pe'(1 + \frac{K_1(Pe'x_f)}{K_0(Pe'x_f)}) \\ \text{Rear wall} \left\{ \begin{aligned} q_v(x_r) &= (T_v - T_a)\lambda_{th}Pe'(-1 + \frac{K_1(Pe'x_r)}{K_0(Pe'x_r)}) \end{aligned} \right. \end{aligned} \right.$$

$q_v$  = heat flow,  $T_v$  = evaporation temperature,  $T_a$  = ambient Temperature,  $\lambda_{th}$  = thermal conductivity,  $Pe'$  = modified Peclet number,  $K_0, K_1$  are modified Bessel number of second kind and zeroth, first order respectively  
 $x_f$  and  $x_r$  are x-coordinates of front and rear wall respectively

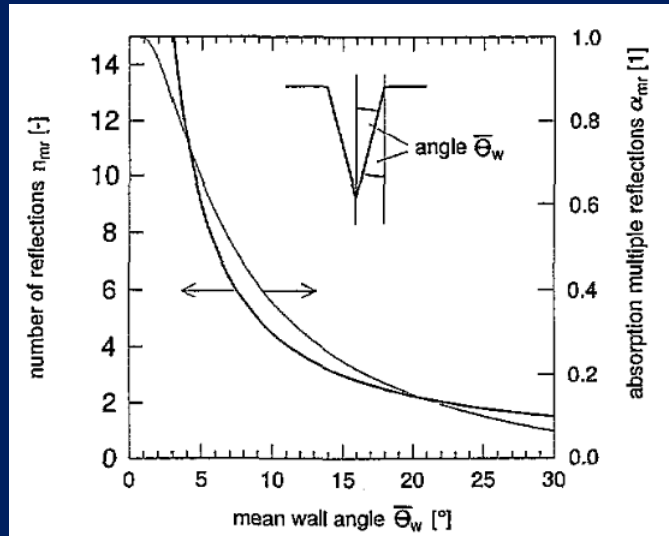
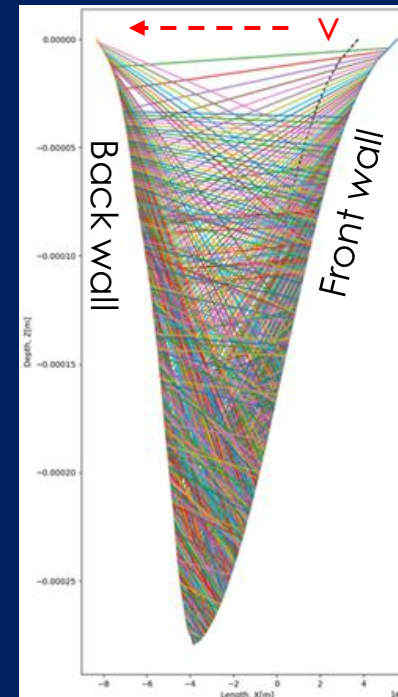


Figure 3. Number of reflections  $n_{mr}$  (thick line) and corresponding absorption coefficient  $\alpha_{mr}$  (thin line) dependent on the mean wall angle  $\bar{\theta}_w$ .

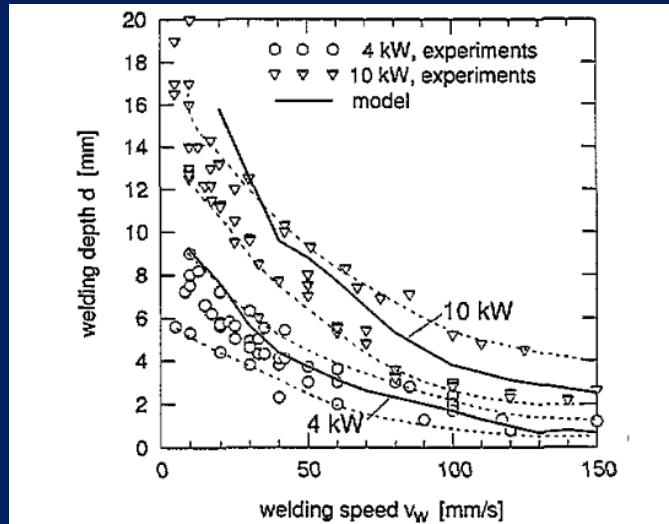


Figure 4. Comparison of welding depth  $d$  versus welding speed  $v_w$  with experiments for 4 and 10 kW laser power.

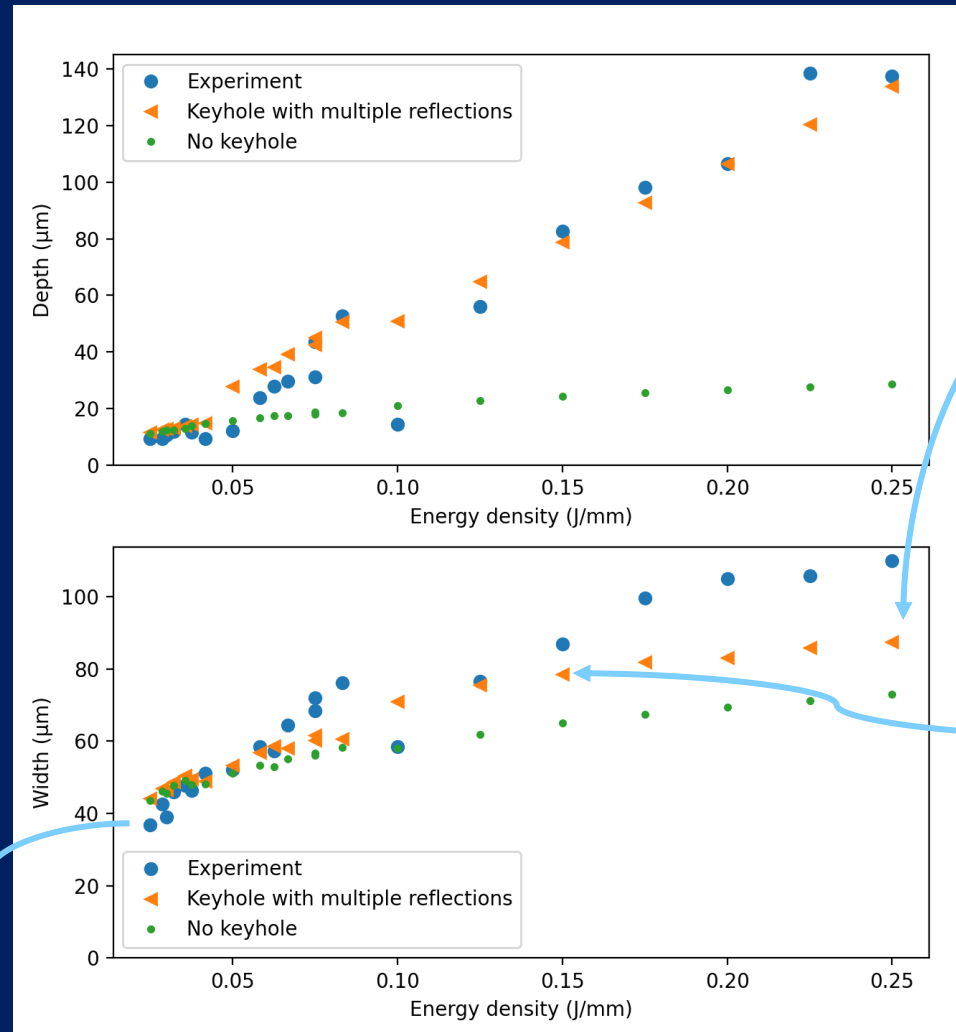
# Keyhole Model - Effect of Multiple Reflections

Multiple reflections from Kaplan model implemented via Jahn's analytical model.

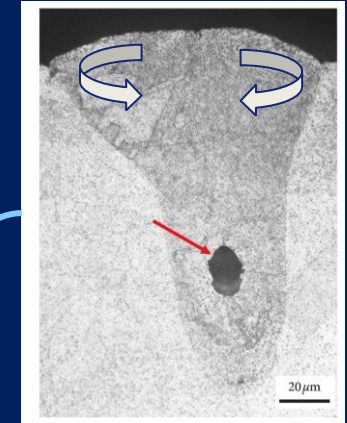
This strategy allows for computation of a keyhole shape, including multi reflections, without a full ray tracking algorithm

**Experiment vs simulation trend is overall great!**

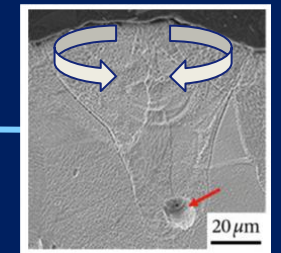
Fluid flow is required to perfectly capture the width at higher energy density (discussed later)



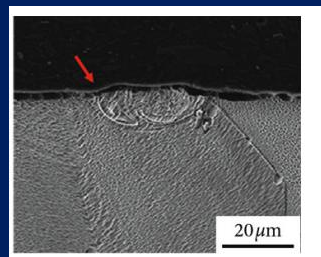
ED=0.25 (100/400)



ED=0.15 (60/400)



ED=0.03 (60/2400)



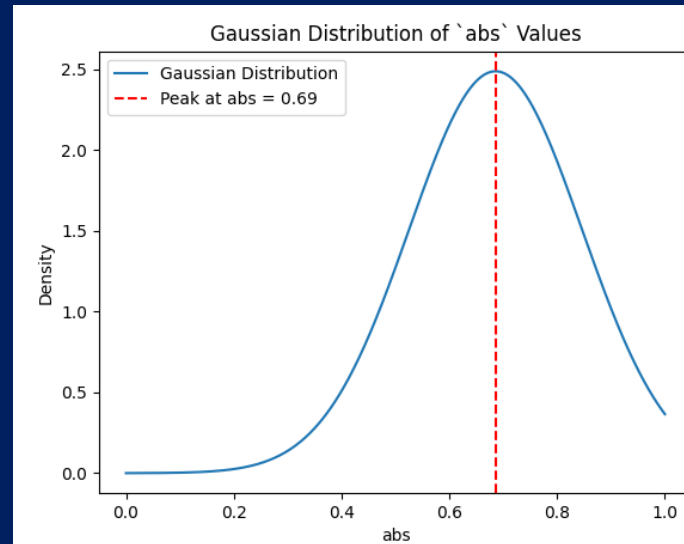
1. A. Kaplan, A model of deep penetration laser welding based on calculation of the keyhole profile. J. Phys. D. Appl. Phys. 27, 1805–1814 (1994)
2. Jahn, M., & Montalvo-Urquiza, J. (2020). Modeling and simulation of keyhole-based welding as multi-domain problem using the extended finite element method. Applied Mathematical Modelling, 82, 731–747
3. Jun Wei et al. Formation of SS316L Single Tracks in Micro Selective Laser Melting Advances in Materials Science and Engineering Volume 2019

# Full ray tracing model – available from 2025b

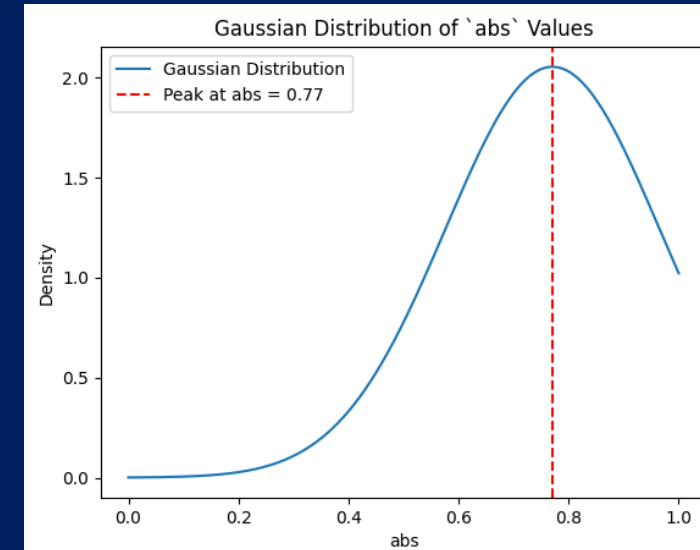
Analytically the full ray tracing means we account for a probabilistic function for effect on absorptivity of the alloy

Case shown from Ti64 where probability function shows the density of reflected rays which peak at ~77% absorptivity at a higher energy parameter whereas at ~69% absorptivity for a lower energy parameter.

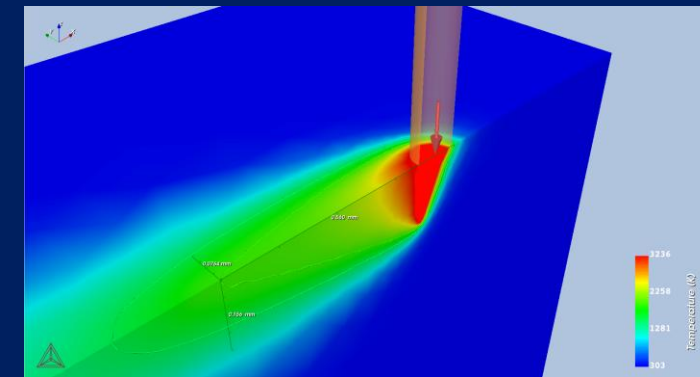
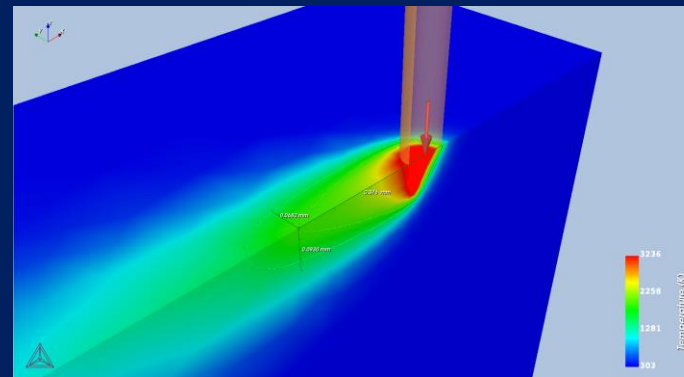
This shows there is a shape/size factor of melt pool to how much reflection a laser beam would produce. Of course there will always be regions where there is 100% reflections but they are less frequent



P 100 W v 500 mm/s for Ti64



P 150 W v 500 mm/s for Ti64



Simulation done in Thermo-Calc 2025b development

# Fluid flow model

# Fluid flow

To account for fluid flow, we add a fluid transport term to heat-flow equation (Eqn.1)

$$\frac{\dot{H}_m}{V_m} = \text{div}(\kappa \text{grad}(T)) - \frac{v}{V_m} \text{grad}(H_m) + \dot{Q}$$

Where  $v$  is the velocity vector field and maybe imposed or obtained from Navier-Stokes equation:

$$\rho \dot{v} + \rho(v \text{grad})v - \mu(\text{divgrad})v = F_v - \text{grad}P$$

$\mu$  is the viscosity,  $F_v$  is volume force, e.g. gravitational force and  $P$  is internal pressure (pressure in chamber)

*This equation also assumes that liquid is incompressible.*

$\rho$  refers to the density; that can be approximated as:

$$\rho = \frac{1}{V_m} \sum_k x_k M_k$$

$M_k$  is molar weight in kg/mol

1. Smagorinsky, J. (1963). General circulation experiments with the primitive equations: I. The basic experiment. Monthly Weather Review, 91(3), 99–164

# Fluid flow

## Smagorinsky constant

We use a subgrid model based on [Smagorinsky,1963] to treat large eddy simulations in fluid flow. It relies on eddy-viscosity assumption that is applied to unresolved turbulent motions that cannot be directly simulated due to computational limitations.

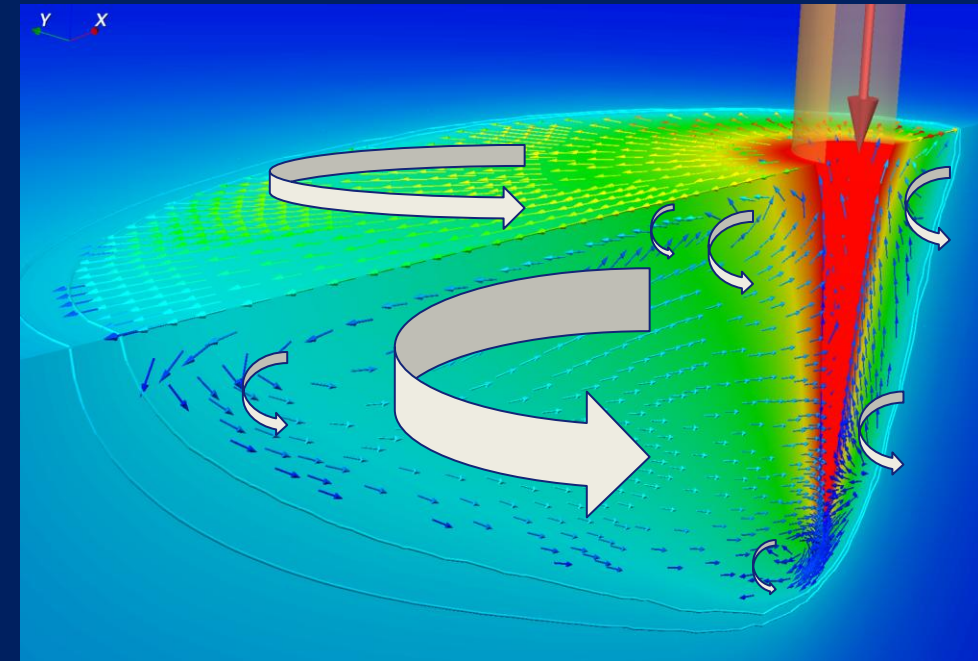
So this model is a simple way to estimate subgrid-scale (SGS) viscosity in large eddy simulations as

$$\nu_{SGS} = (C_S \Delta)^2 |\bar{S}|$$

Where,  $C_S$  = Smagorinsky constant (default=0.18),  $\Delta$ = filter width (length scale),  $|\bar{S}|$ = magnitude of resolved strain rate tensor

In some cases, fluids with higher flow rates + low viscosity, a larger Smagorinsky constant is applied

An example is shown for an Al-alloy



Melt pool for AlSi10Mg alloy with an increased Smagorinsky constant (0.5 instead of 0.18)

1. Smagorinsky, J. (1963). General circulation experiments with the primitive equations: I. The basic experiment. Monthly Weather Review, 91(3), 99–164

# Fluid flow : Marangoni flow

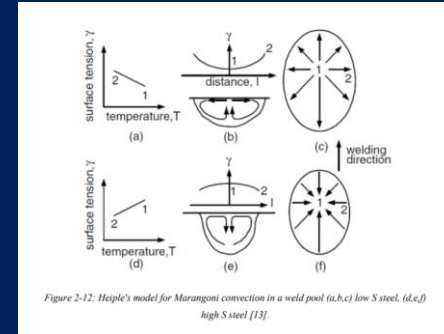
The most important boundary condition in Navier-Stokes setup is the Marangoni boundary condition that reflects the tangential force on the surface of the melt pool due to temperature variation of surface tension or the so-called Marangoni effect.

In AM, large temperature gradients on the surface of the melt pool, leads to the Marangoni effect and is the primary cause of convective flow inside the melt pool.

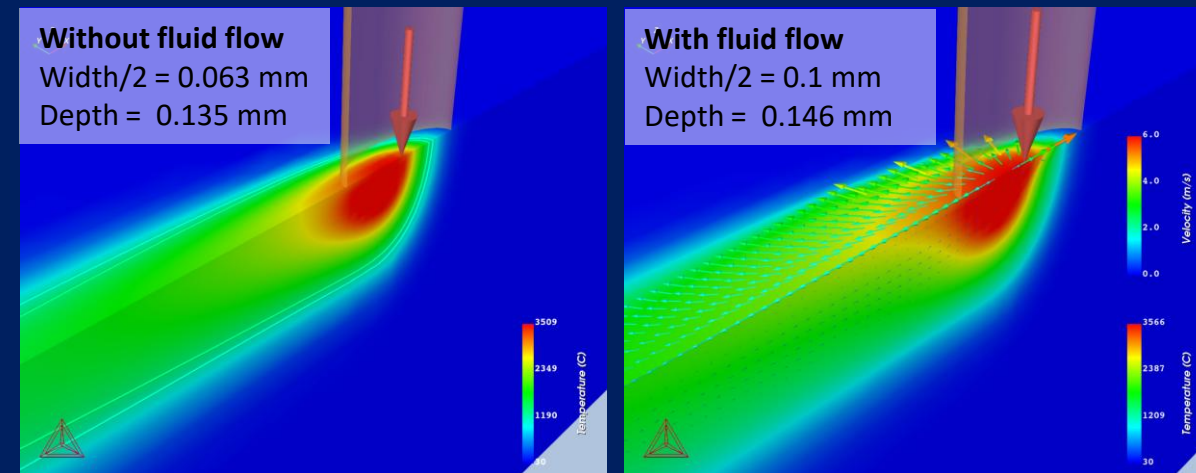
The Marangoni shear stress ( $\tau$ ) is modeled using the following equation:

$$\tau = \frac{\partial \gamma}{\partial T} \nabla_s T$$

Where  $\gamma$  is the surface tension,  $\nabla_s$  is the tangential component of the spatial derivative



Kou, S., Welding metallurgy, second edition. 2002: Wiley978-0-471-43491-7



Single point melt pool for IN738 calculated at 230 W, 960 mm/s with and without fluid flow [Grange et al., 2021]

# Example on validation of Keyhole & fluid flow

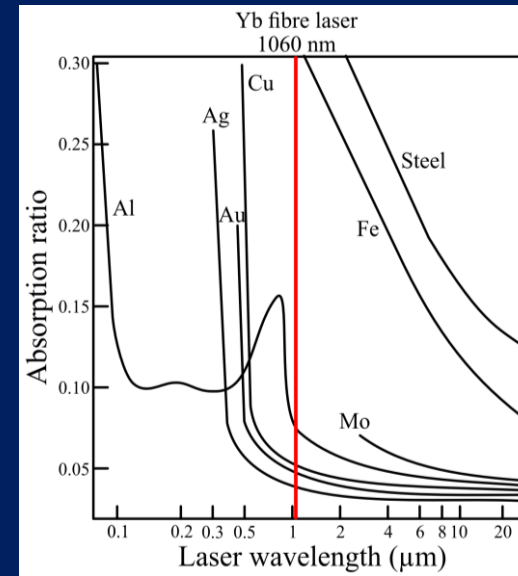
- Experimental data from Hu, Z., Nagarajan, B., Song, X., Huang, R., Zhai, W., & Wei, J. (2019). Formation of SS316L Single Tracks in Micro Selective Laser Melting: Surface, Geometry, and Defects. *Advances in Materials Science and Engineering*, 2019
- 316L alloy from materials library

# Absorptivity model

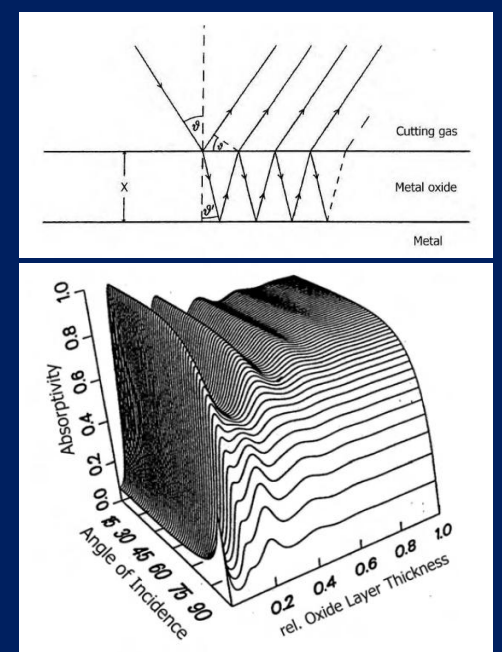
# Absorptivity model

Absorptivity of a flat metal surface is function of

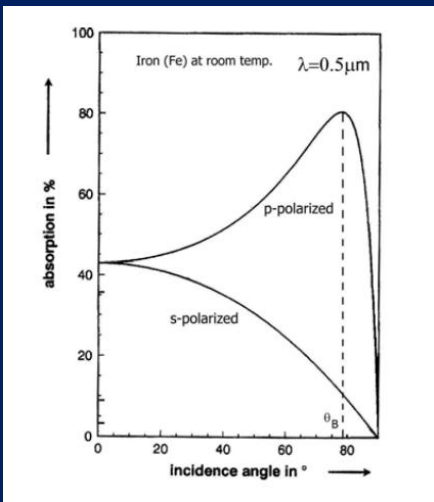
- Alloy composition
- Wavelength of heat source
- Temperature
- Angle of incidence of heat source
- Oxide layer thickness
- Etc..



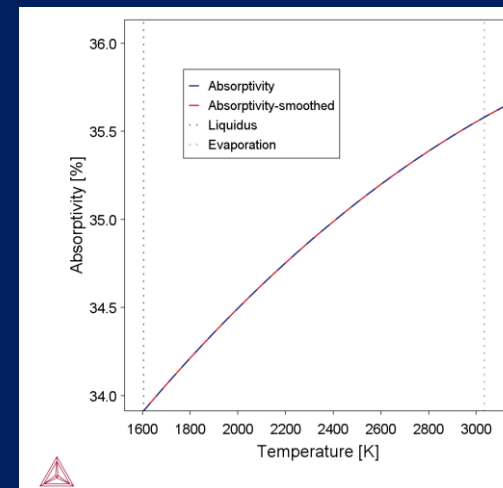
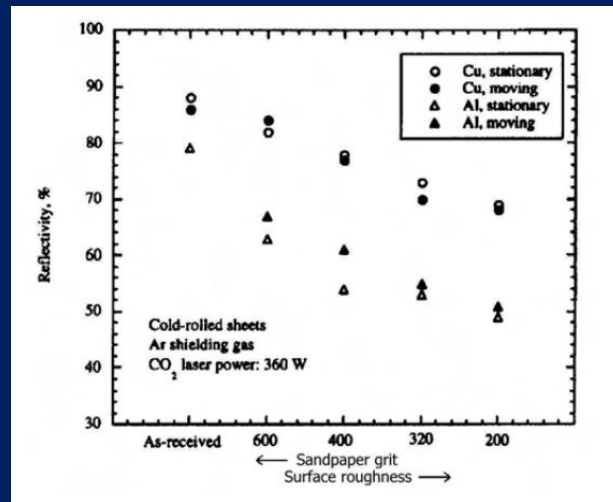
Variation of absorptivity with laser wavelength [based on Drude model]



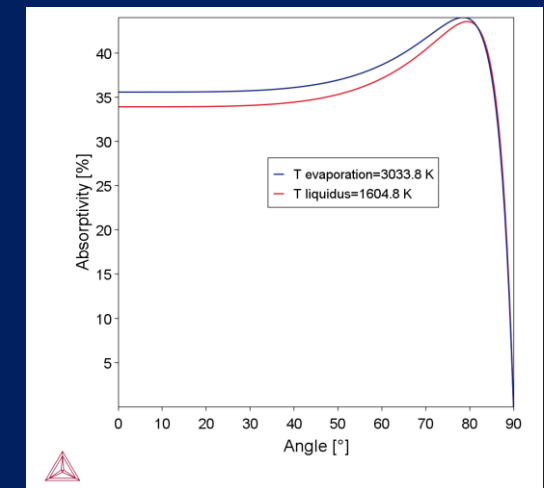
Variation of absorptivity with oxide thickness [taken from Bergström, 2005]



Variation of absorptivity with light polarisation and surface roughness of sample [taken from Bergström, 2005]



Variation of absorptivity with temperature and incidence angle of laser



1. Prokhorov A.M., Konov V.I., Ursu I., Mihailescu I.N., "Laser Heating of Metals", The Adam Hilger Series on Optics and Optoelectronics, 1990, ISBN 0-7503-0040-X
2. Bergström, D. (2005). The Absorptance of Metallic Alloys to Nd: YAG and Nd: YLF Laser Light

# Absorptivity model

Based on Lorentz-Drude model and Yang et al., 2021 wherein refractive index  $\tilde{n} = \sqrt{\tilde{\epsilon}}$  for nonmagnetic mediums

$$\tilde{\epsilon} = \epsilon_r + i\epsilon_i$$

$$\epsilon_r = 1 - \frac{\omega_p^2}{f_L^2 + \gamma^2}, \quad \epsilon_i = \frac{\gamma}{f_L} \cdot \frac{\omega_p^2}{f_L^2 + \gamma^2}$$

Where  $\epsilon_r$  and  $\epsilon_i$  are the real and imaginary components of electric permittivity.  $f_L$  = laser frequency,  $\gamma$  = damping frequency,  $\omega_p$  is the plasma frequency

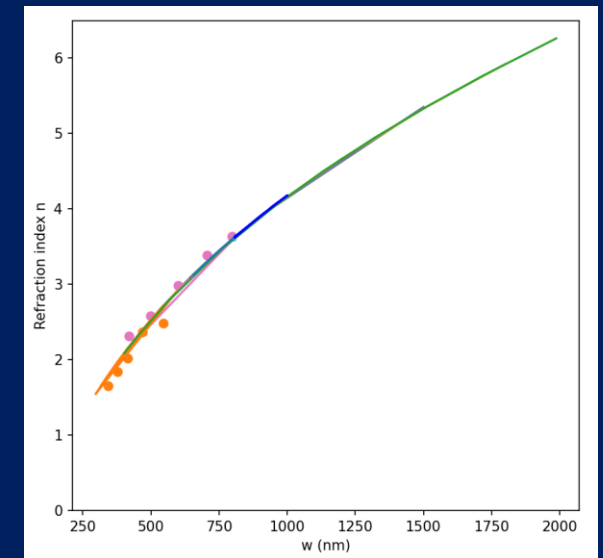
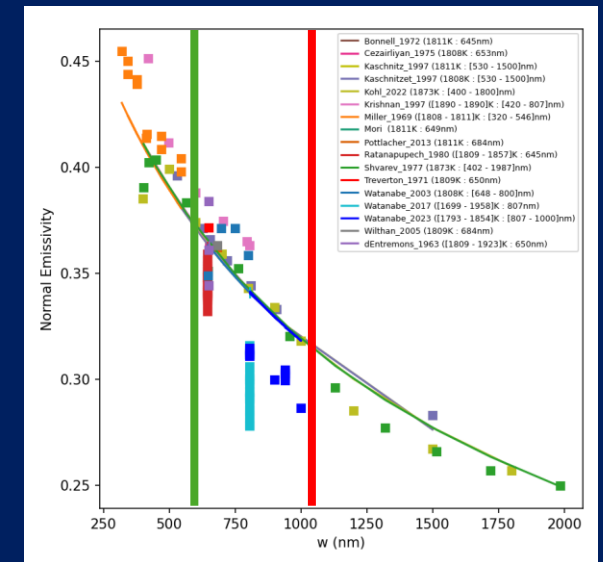
$$\omega_p = \sqrt{\frac{N_e q_e^2}{m_e \epsilon_0}}$$

Where  $N_e$  is number density of free electrons,  $q_e$  is absolute value of elementary charge,  $m_e$  is electron mass and  $\epsilon_0$  is vacuum permittivity

$$\gamma = \omega_p^2 \cdot \epsilon_0 \cdot \rho(T)$$

Where  $\rho(T)$  is electrical resistivity

Thus, we can relate refractive index to laser frequency, electrical resistivity and free electron density



Relationship between emissivity (absorptivity), refractive index to wavelength of laser (pure Fe)

1. Yang, Z., Bauereiß, A., Markl, M., & Körner, C. (2021). Modeling Laser Beam Absorption of Metal Alloys at High Temperatures for Selective Laser Melting. Advanced Engineering Materials, 23(9)

# Absorptivity model

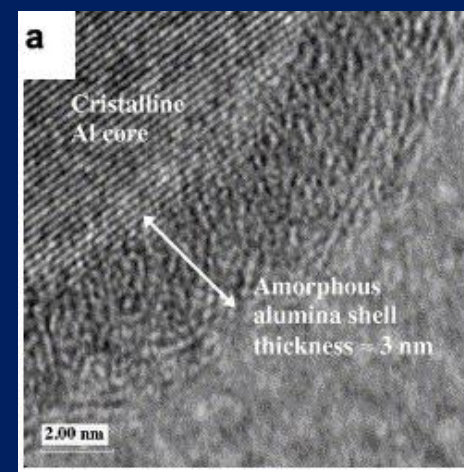
## Additional considerations

For metal powder, interactions are complex.

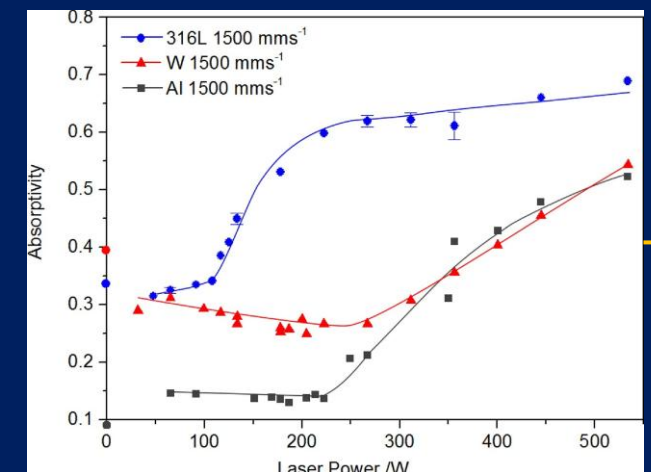
- Metallic powders are oxidised at surface where thin layer of oxide often increases absorptivity. Multiple reflections due to inter-particle dispersion can also cause increased absorptivity
- This is why we provide an absorptivity prefactor over the calculated value

Our treatment *simplifies* the metal as an ideal flat surface of the liquid phase after the powder has melted.

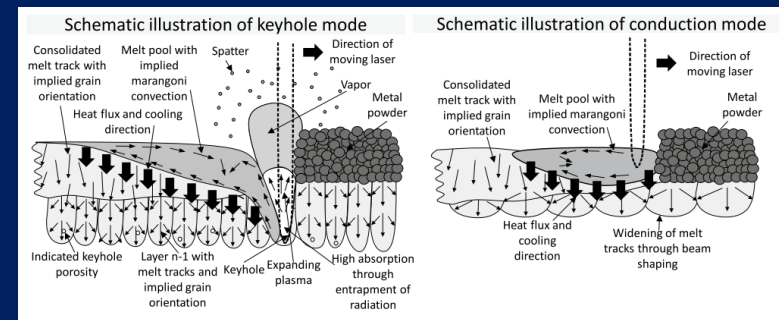
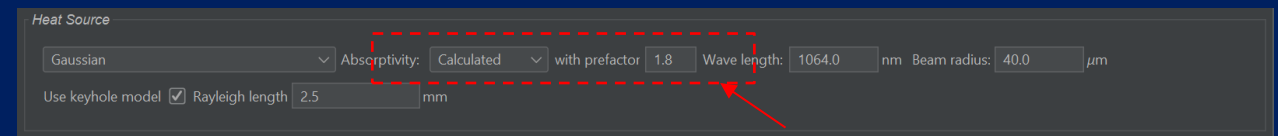
It can be justified at steady-state condition when a melt pool is established and most laser beam hit the liquid surface of the melt pool.



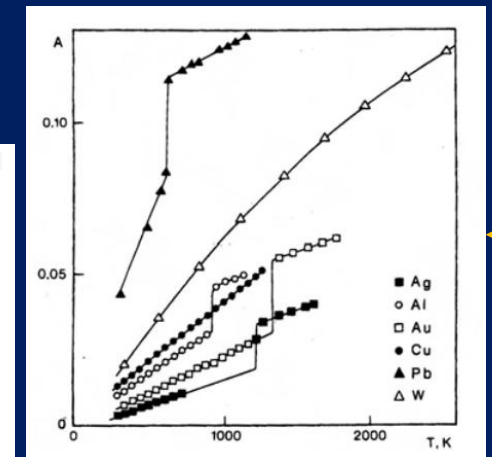
Al<sub>2</sub>O<sub>3</sub> at surface of Al-powder [Rufino et al., 2007]



Effective absorptivity on different metals [Trapp et al., 2017]



Schematic illustration of different laser modes [Stoll et al., 2024]



Laser absorptivity with temperature [Prokhorov, 1990]

1. Rufino, B., Boulc'h, F., Coulet, M.-V., Lacroix, G., & Denoyel, R. (2007). Influence of particles size on thermal properties of aluminium powder. *Acta Materialia*, 55(8), 2815–2827
2. Stoll, T., Prudlik, R., Birg, M., & Wudy, K. (2024). Influence of different beam shapes on melt pool geometry of single melt tracks on IN718. *Progress in Additive Manufacturing*
3. Trapp, J., Rubenchik, A. M., Guss, G., & Matthews, M. J. (2017). In situ absorptivity measurements of metallic powders during laser powder-bed fusion additive manufacturing. *Applied Materials Today*, 9, 341–349
4. Prokhorov A.M., Konov V.I., Ursu I., Mihailescu I.N., "Laser Heating of Metals", The Adam Hilger Series on Optics and Optoelectronics, 1990, ISBN 0-7503-0040-X

# Example on absorptivity model

- Shown with material library for Ni-, Ti-, Fe- and Al- alloys
- Absorptivity and absorptivity v/s incidence angle

# Other considerations for powder bed

When the option “Use separate material properties for powder” is selected, a different thermal conductivity, density and molar volume is used for the powder material as compared to the solid substrate.

The above mentioned properties depend on the porosity ( $\phi$ ) of the powder. The density ( $\rho_{powder}$ ) and molar volume ( $V_{m_{powder}}$ ) of the powder are then simply given as follows:

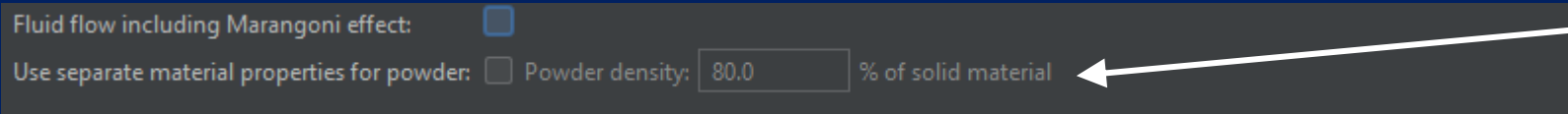
$$\rho_{powder} = \rho_{solid}(1 - \phi)$$

$$V_{m_{powder}} = V_{m_{solid}}\left(\frac{1}{1-\phi}\right)$$

For thermal conductivity of powder, an empirical expression is used which was suggested by Xue and Barlow, 1991.

$$k_{powder} = (6.3 + 22\sqrt{0.09k_{solid} - 0.016}) \frac{k_{solid}(1-\phi)}{\left(\frac{k_{solid}}{k_{air}}\right)(10^{0.523-0.594\phi})-1}$$

Where  $k_{air} = 0.05784$



At the moment, Marangoni and separate powder properties cannot be implemented together

# Other considerations for powder bed

Some other practical consideration in PBF-LB process that are not considered by AM module

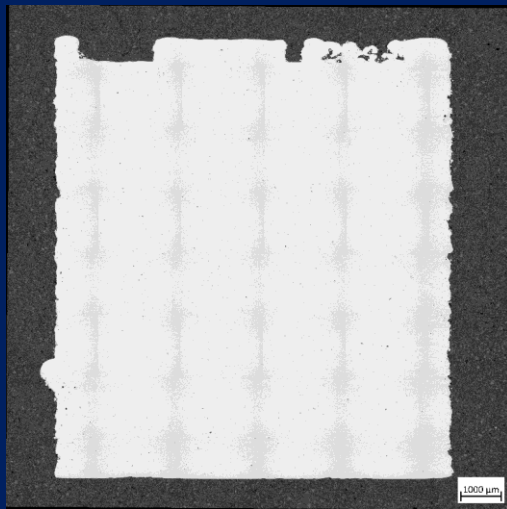
- Gas flow rate: Modifying the gas flow rate to laminar or turbulent (can be partly described by convective heat transfer coefficient)
- Powder bed density: packing density of powder bed changes due to different recoater types, feeding mechanisms and powder size distribution (powder density can partly describe but more description needed)
- Stochastic defects occurring due to spatter, melt pool instabilities, recoater hit etc.

# Printability maps

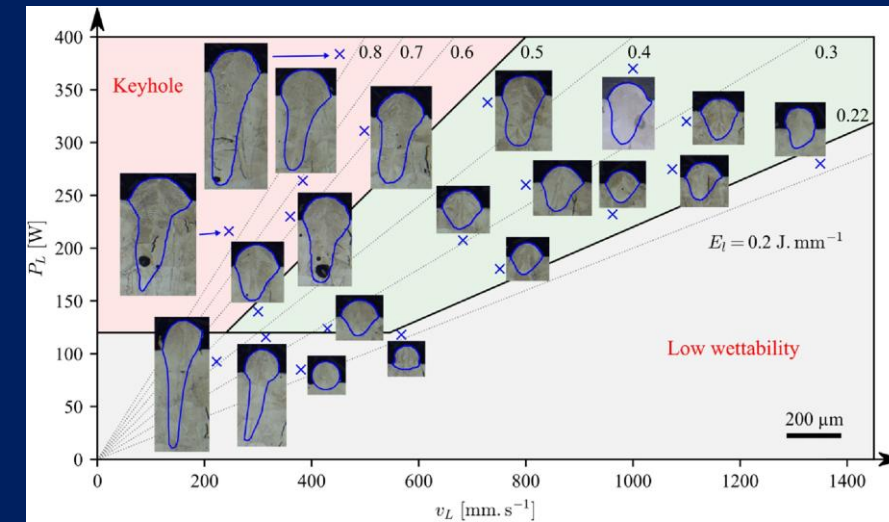
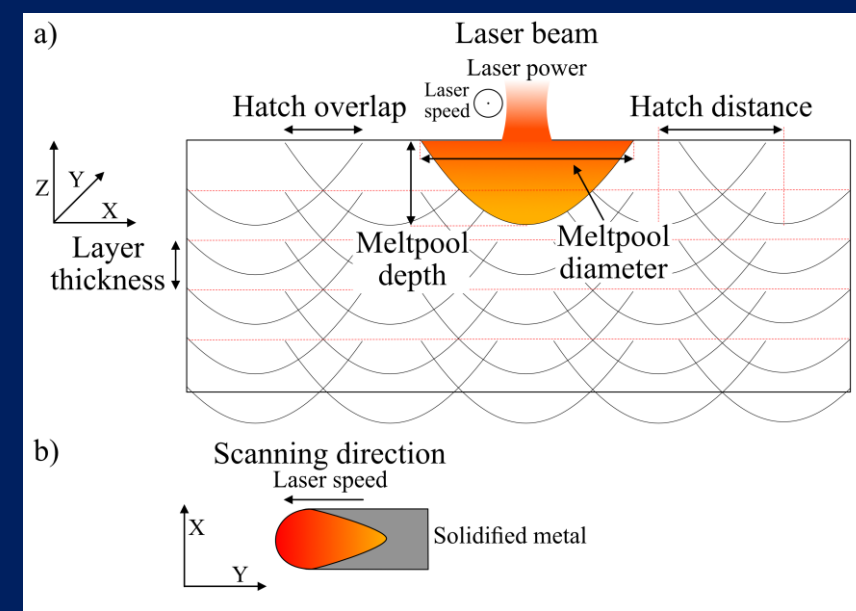
# Printability maps

Understand basic processing parameters:

- Laser power (W)
- Laser speed (mm/s)
- Layer thickness (mm)
- Hatch distance (mm)



Fully dense material (Al-HS1) produced via PBF-LB



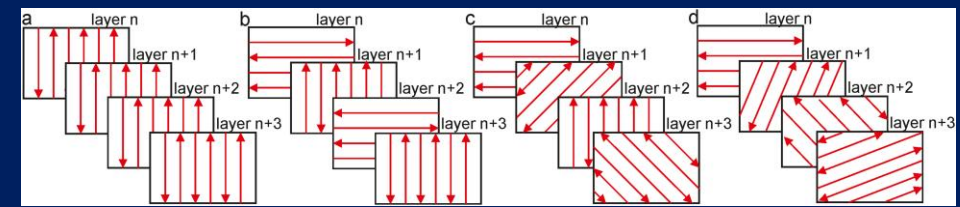
Effect of laser speed ( $v_L$ ) v/s laser power on melt pool [Grange et al., 2021]

1. Grange, D., Queva, A., Guillemot, G., Bellet, M., Bartout, J. D., & Colin, C. (2021). Effect of processing parameters during the laser beam melting of Inconel 738: Comparison between simulated and experimental melt pool shape. Journal of Materials Processing Technology, 289. <https://doi.org/10.1016/j.jmatprotec.2020.116897>

# Printability maps

And advanced processing parameters:

- Scan rotation
- Stripe width
- Skywriting
- Beam shaping (in 2025b)
- And more..



Scan rotation (0, 90, 45, 67) [Leicht et al., 2020]

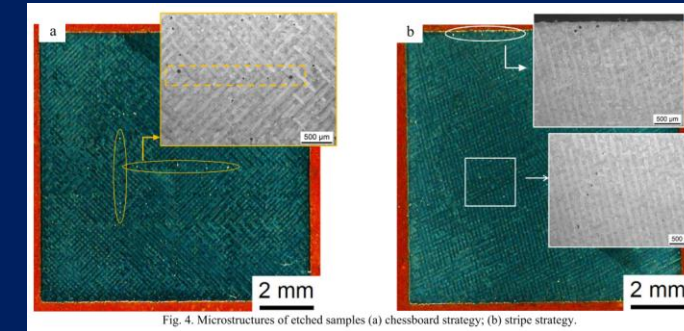
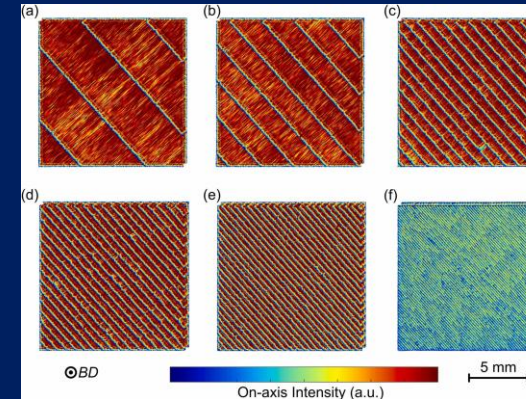
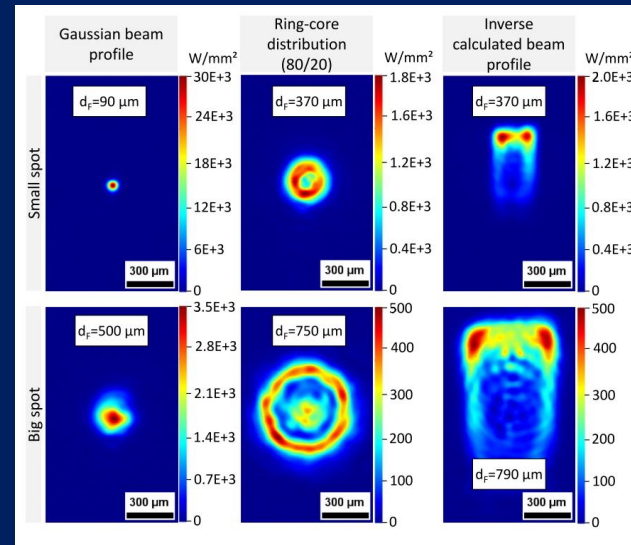


Fig. 4. Microstructures of etched samples (a) chessboard strategy; (b) stripe strategy.

Chessboard and stripe scanning strategy [Mancisidor et al., 2016]

Stripe width (5 mm, 2.5 mm, 1 mm and 0.7 mm) [Fardan et al., 2025]



Beam shaping [Stoll et al., 2024]

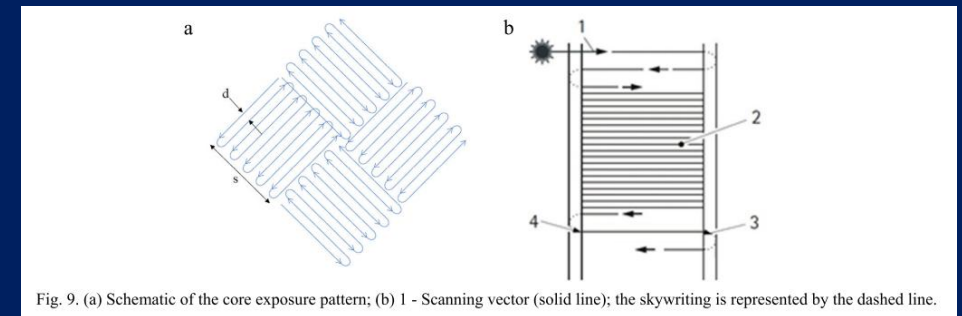


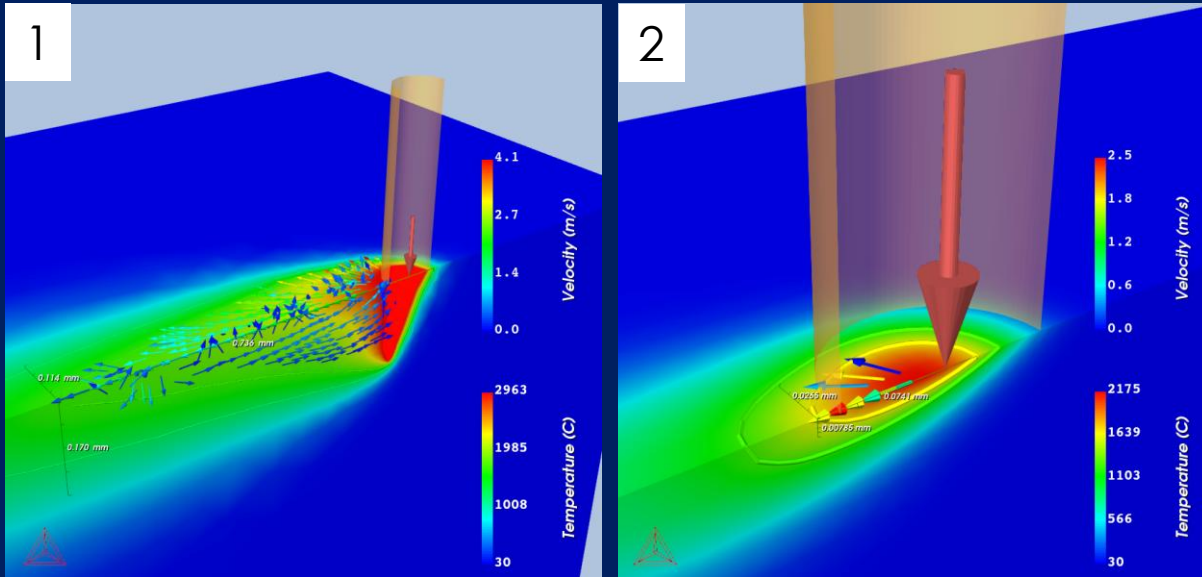
Fig. 9. (a) Schematic of the core exposure pattern; (b) 1 - Scanning vector (solid line); the skywriting is represented by the dashed line.

Core exposure scanning and skywriting [Mancisidor et al., 2016]

1. Stoll, T., Prudlik, R., Birg, M., & Wudy, K. (2024). Influence of different beam shapes on melt pool geometry of single melt tracks on IN718. *Progress in Additive Manufacturing*
2. Mancisidor, A. M., Garcíandia, F., Sebastian, M. S., Álvarez, P., Díaz, J., & Unanue, I. (2016). Reduction of the residual porosity in parts manufactured by selective laser melting using skywriting and high focus offset strategies. *Physics Procedia*, 83, 864–873. <https://doi.org/10.1016/j.phpro.2016.08.090>
3. Fardan, A., Fazi, A., Schröder, J., Mishurova, T., Deckers, T., Bruno, G., Thuvander, M., Markström, A., Brodin, H., & Hryha, E. (2025). Microstructure tailoring for crack mitigation in CM247LC manufactured by powder bed fusion – Laser beam. *Additive Manufacturing*, 99, 104672. <https://doi.org/10.1016/j.addma.2025.104672>
4. Leicht, A., Yu, C. H., Luzin, V., Klement, U., & Hryha, E. (2020). Effect of scan rotation on the microstructure development and mechanical properties of 316L parts produced by laser powder bed fusion. *Materials Characterization*, 163. <https://doi.org/10.1016/j.matchar.2020.110309>

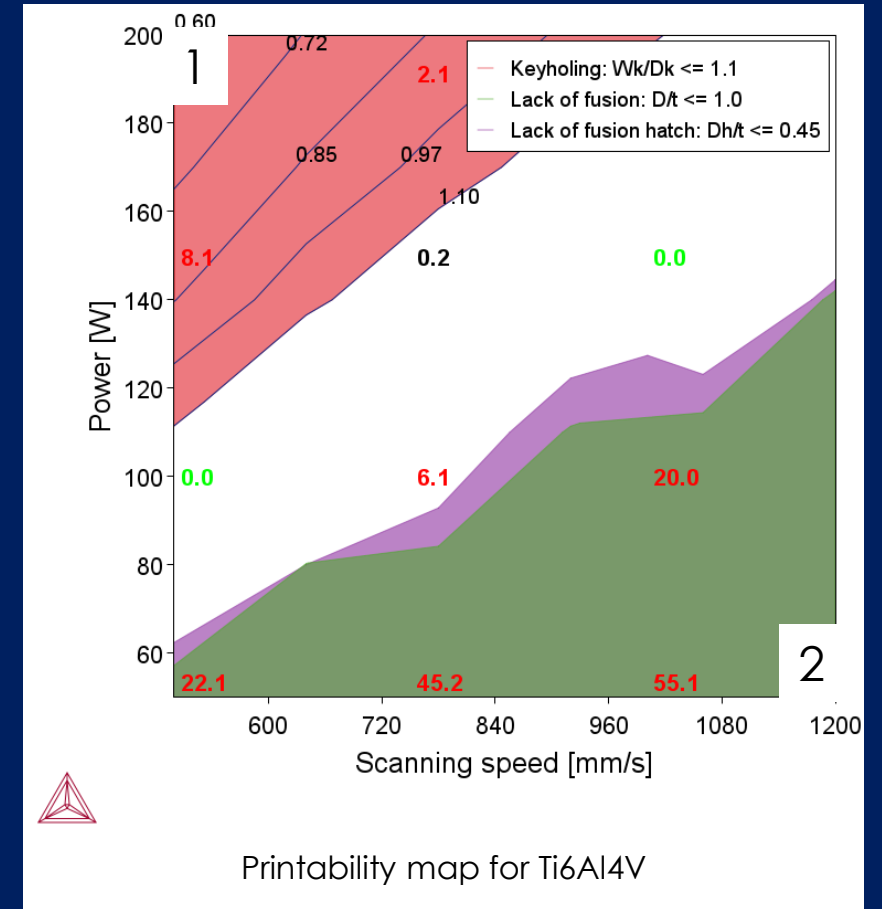
# Printability maps

Printability to avoid defects (lack of fusion, keyhole control and good overlaps)



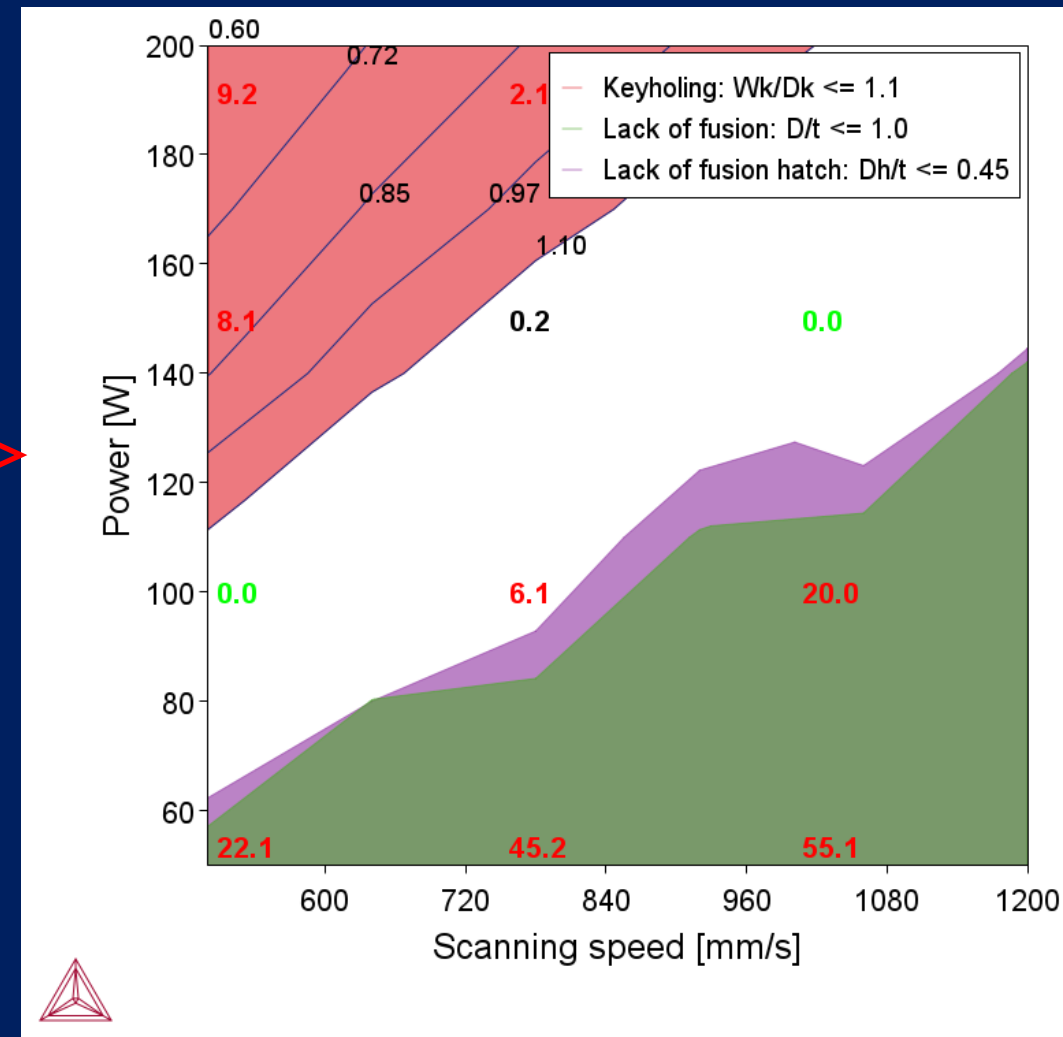
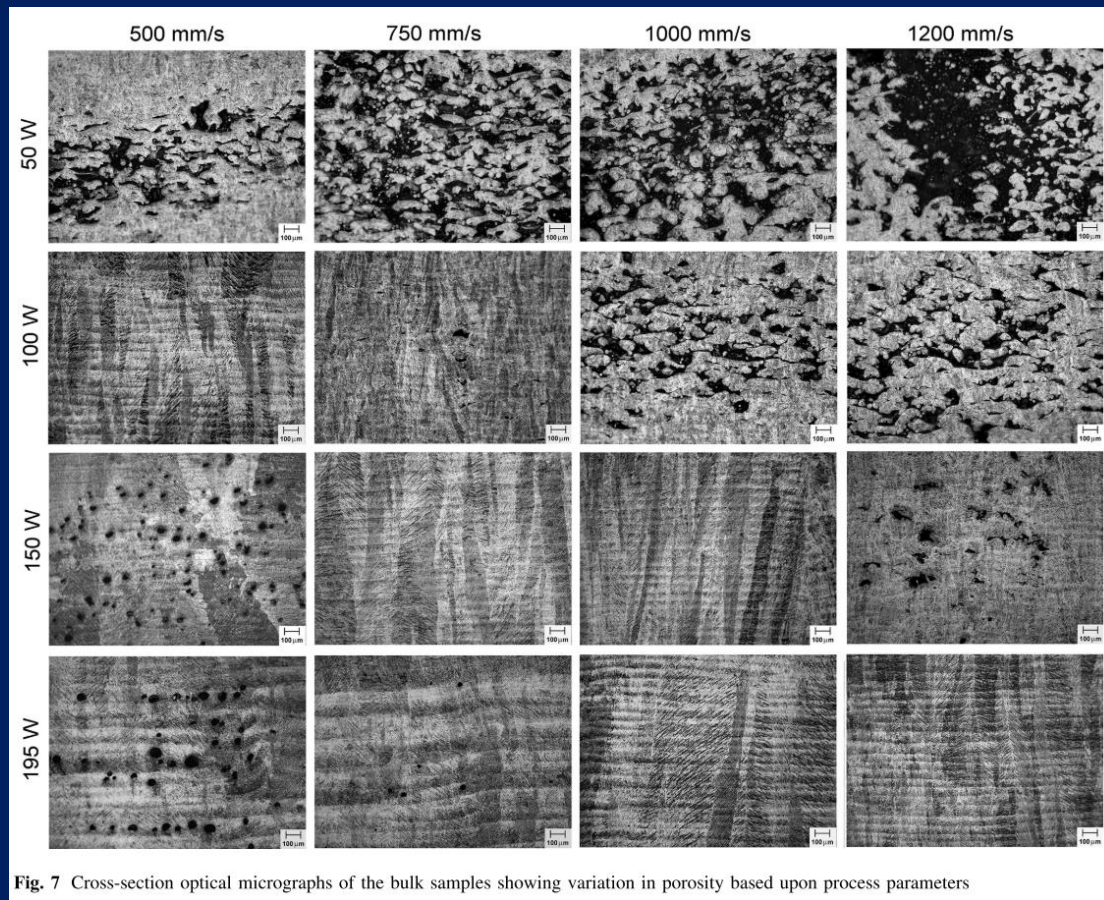
High power low speed melt pool  
Ti64 alloy simulation on 25a

Low power high speed melt pool  
Ti64 alloy simulation on 25a



Printability map for Ti6Al4V

# Printability maps



Dilip et al., 2017 conducted single track and then made processability maps to overlay porosity over process parameter

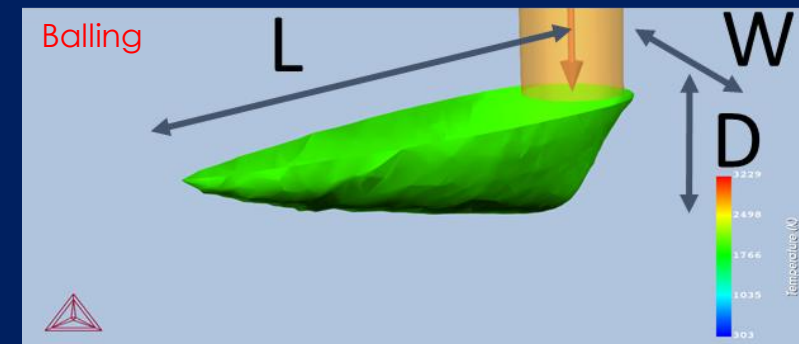
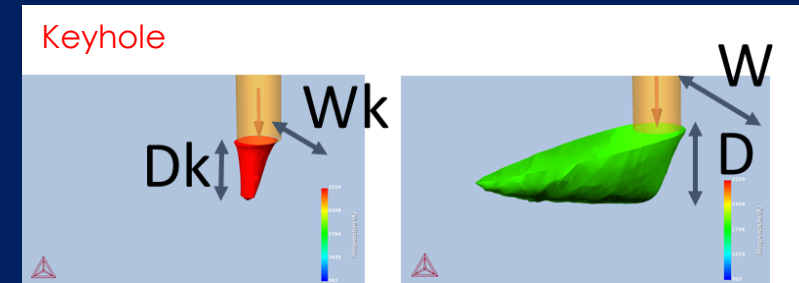
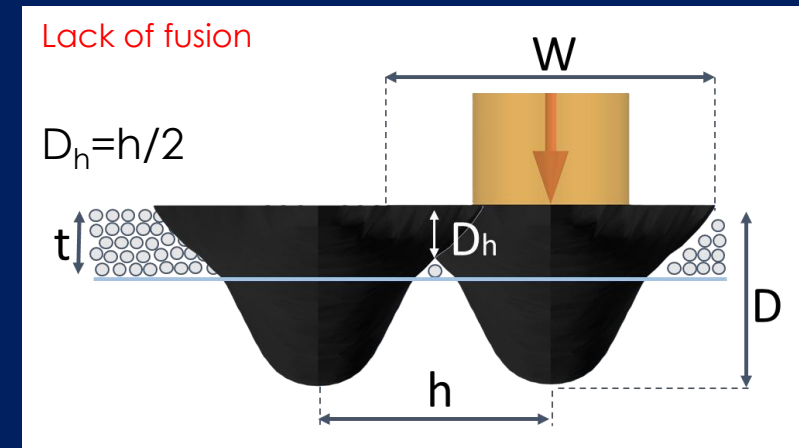
1. Dilip, J. J. S., Zhang, S., Teng, C., Zeng, K., Robinson, C., Pal, D., & Stucker, B. (2017). Influence of processing parameters on the evolution of melt pool, porosity, and microstructures in Ti-6Al-4V alloy parts fabricated by selective laser melting. Progress in Additive Manufacturing, 2(3), 157–167. <https://doi.org/10.1007/s40964-017-0030-2>

# Printability maps

- Printability (or processability) maps provides a processing window for the alloy in concern. Which parameters provide fully bonded material (without defects)
- Thermo-Calc plots it as a grid plot with functions namely keyholing, balling, lack of fusion etc. against process parameters (laser speed, hatch distance etc.) as axis variable
- Done as steady-state calculation
- Provides the user to translate melt pool dimensions to relate to printing defects common in AM processes
- Stochastic defects, spatter defects are not possible to simulate

Lack of fusion:	$\frac{D}{t}$	( $<1$ )
Lack of fusion (hatch):	$\frac{D_h}{t}$	( $<0.8$ )
Keyhole criteria:	$\frac{W_k}{D_k}$ or $\frac{W}{D}$	( $<1.1$ )
Balling criteria:	$\frac{D}{L}$ or $\frac{W}{L}$	( $\ll 1$ )

Note: Values in red are based on literature [1-3]. User may input other values for better fit

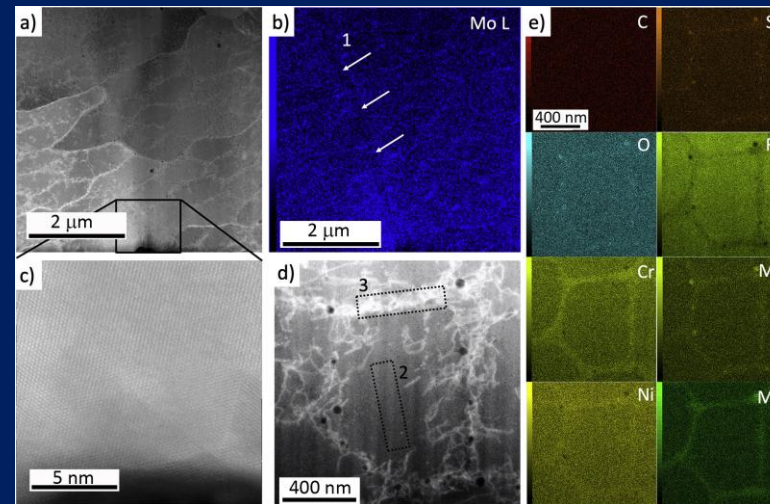
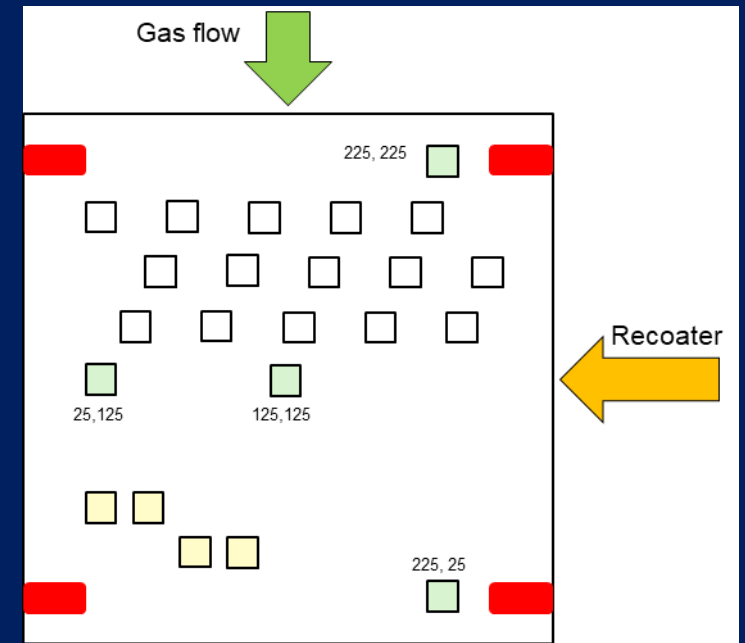


Lack of fusion, keyhole and balling criterion

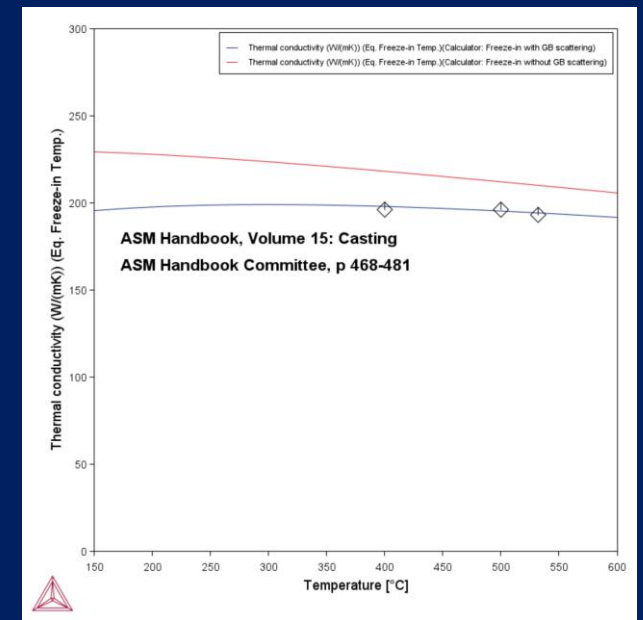
1. Hu, Z., Nagarajan, B., Song, X., Huang, R., Zhai, W., & Wei, J. (2019). Formation of SS316L Single Tracks in Micro Selective Laser Melting: Surface, Geometry, and Defects. *Advances in Materials Science and Engineering*, 2019(Article ID 9451406), 1–9. <https://doi.org/10.1155/2019/9451406>
2. Johnson, L., Mahmoudi, M., Zhang, B., Seede, R., Huang, X., Maier, J. T., Maier, H. J., Karaman, I., Elwany, A., & Arróyave, R. (2019). Assessing printability maps in additive manufacturing of metal alloys. *Acta Materialia*, 176, 199–210. <https://doi.org/10.1016/j.actamat.2019.07.005>
3. Katagiri, J., Kusano, M., Minamoto, S., Kitano, H., Daimaru, K., Tsujii, M., & Watanabe, M. (2023). Melt Pool Shape Evaluation by Single-Track Experiments and Finite-Element Thermal Analysis: Balling and Lack of Fusion Criteria for Generating Process Window of Inconel738LC. *Materials*, 16(4), 1729. <https://doi.org/10.3390/ma16041729>

# Further work on printability maps

- Working together with Centre for Additive Manufacturing-Metal at Chalmers University of Technology, Sweden
- Study conducted in EOS M290 for 316L stainless steel and Al-HS1 (Al-alloy). Both have microsegregation in solidification structures, will work as good validation for phase interface scattering
- Print small cube samples without scan rotation to validate melt pool dimensions and overlay with printability maps. Both will be conducted experimentally and validated via AM module
- Results planned to be presented at EuroPM, 2025 at Glasgow in September 2025



Solidification microstructure of 316L produced by PBF-LB [Godec et al., 2020]

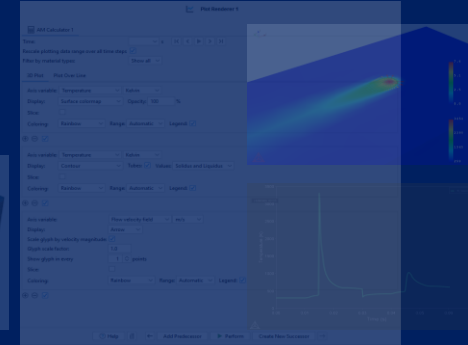
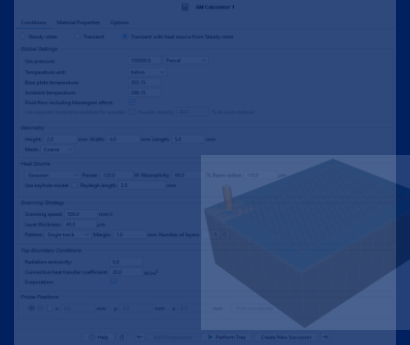
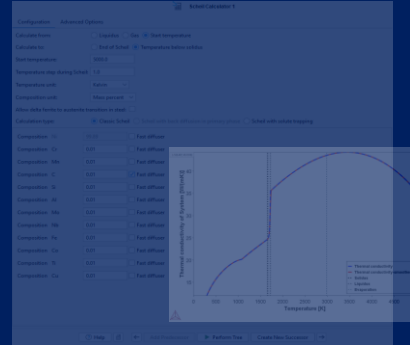


1. Godec, M., Zaeferrer, S., Podgornik, B., Šinko, M., & Tchernychova, E. (2020). Quantitative multiscale correlative microstructure analysis of additive manufacturing of stainless steel 316L processed by selective laser melting. *Materials Characterization*, 160. <https://doi.org/10.1016/j.matchar.2019.110074>

# Questions?

Short break for 15 minutes ☺

# Unified Treatment of Material Properties and Process Parameters



Precipitation



Property Model



Diffusion

System Definer

Extended Scheil  
Calculation

AM Module

Post processing

Export results

Define alloy system, retrieve Thermodynamic and Thermophysical data

Extraction of materials properties from evaporation down to RT including solidification segregation.

Obtain enthalpy, heat capacity, density, thermal conductivity, viscosity, surface tension, volume, molar mass of Gas and driving force for evaporation

Simulate AM with parameters such as: Laser power, Scanning speed and Strategy Layer thickness, Base plate temperature.

Takes into account: Thermal conduction and Fluid flow, Powder density, and heat losses due to radiation and convection and evaporation

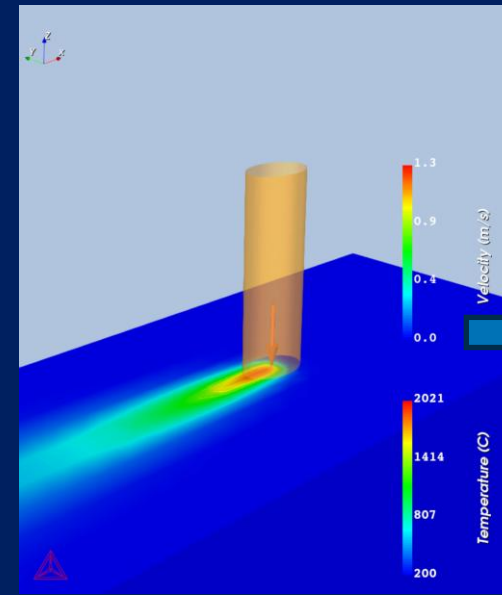
Visualize in 3D, over a selected line or at a chosen point over time.

Plottable quantities: Temperature, Flow velocity, Surface tension, Thermal conductivity, Dynamic viscosity and Melt Pool dimension.

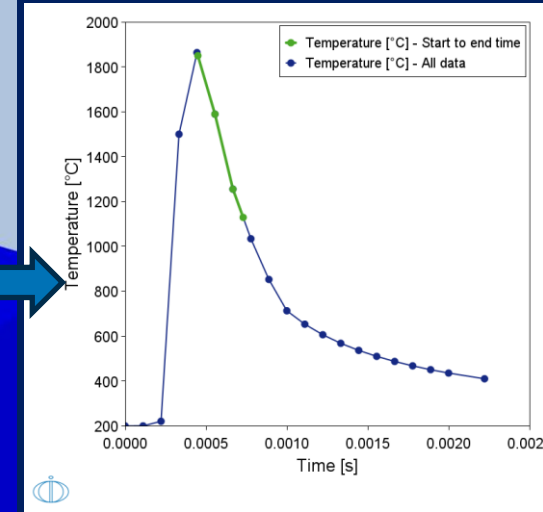
Export time-temperature profile, melt pool dimension and/or temperature distribution in space to other Thermo-Calc modules like DICTRA or PRISMA, or to other external computational softwares.

# Advanced setup (AM → DICTRA)

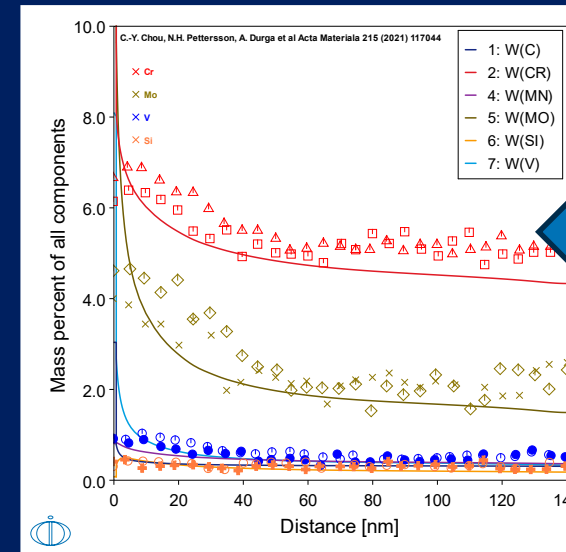
- Available as AM\_05 example with the software
- We simulated the melt pool from Chou et al., 2021 as a single track transient calculation
- Calculation with Transient with HS from steady state
- Took the probe information from AM calculator → DICTRA to define non isothermal condition from Liquid → FCC solidification
- This provided the chemical composition at solidification boundary, showing a good relation to their experimental results



Single track on Fe-alloy



Input to DICTRA from probe time-temperature profile



Microsegregation profile overlaid with DICTRA composition profile

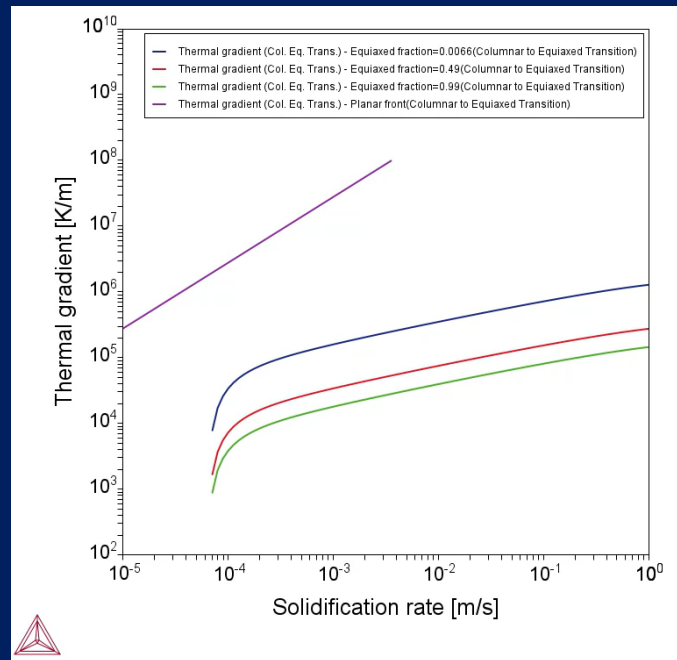
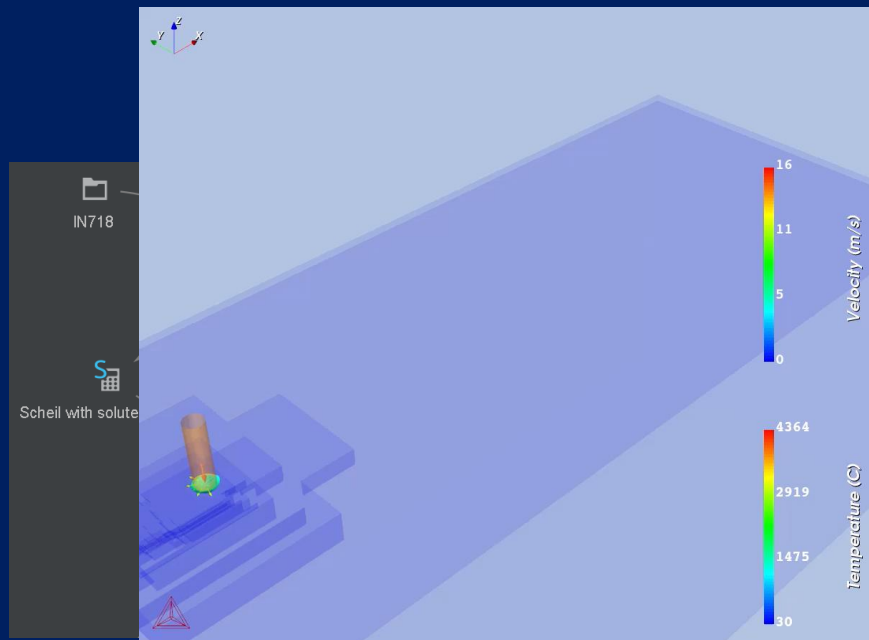


DICTRA moving interface setup

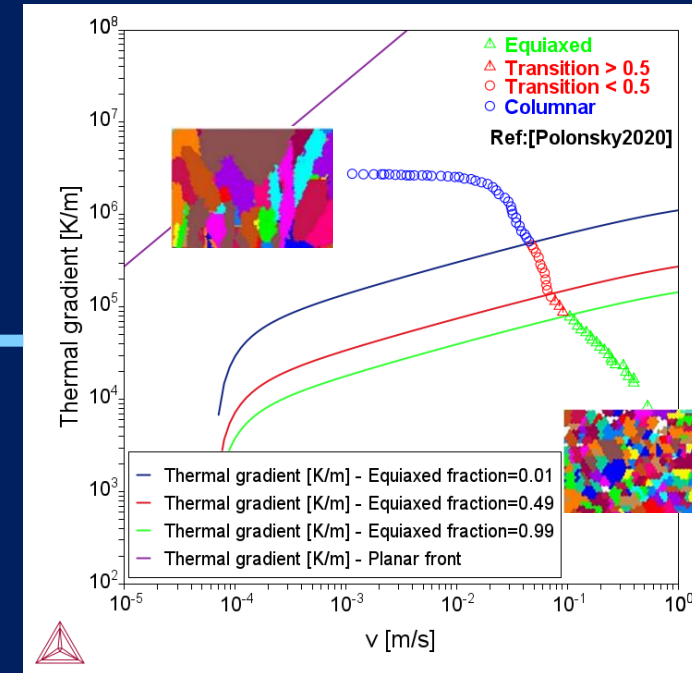
1. Chou, C.-Y., Pettersson, N. H., Durga, A., Zhang, F., Oikonomou, C., Borgenstam, A., Odqvist, J., & Lindwall, G. (2021). Influence of solidification structure on austenite to martensite transformation in additively manufactured hot-work tool steels. *Acta Materialia*, 215, 117044. <https://doi.org/10.1016/j.actamat.2021.117044>

# Advanced setup (AM → CET model)

- Similar to AM\_10 example with the software
- Available as a General Property model in Thermo-Calc. Based on Polonsky et al.2020 which shows regions with 0.01, 0.49 and 0.99 equiaxed grain fraction for IN718 alloy printed via PBF-EB process
- Users can plot AM calculations and combine with CET model to know if the melt pool solidifies with columnar or requiaxed grains



CET model example G\_17



IN718 transient calculation (P 250W , v 1000 mm/s) overlaid on CET model AM\_10

Polonsky, A. T., Raghavan, N., Echlin, M. P., Kirka, M. M., Dehoff, R. R., & Pollock, T. M. (2020). 3D Characterization of the Columnar-to-Equiaxed Transition in Additively Manufactured Inconel 718. In *Superalloys 2020* (pp. 990–1002). [https://doi.org/10.1007/978-3-030-51834-9\\_97](https://doi.org/10.1007/978-3-030-51834-9_97)

# Advanced setup (Calibrating HS)

What to do if you have experimental alloy and/or experimental machine setup?

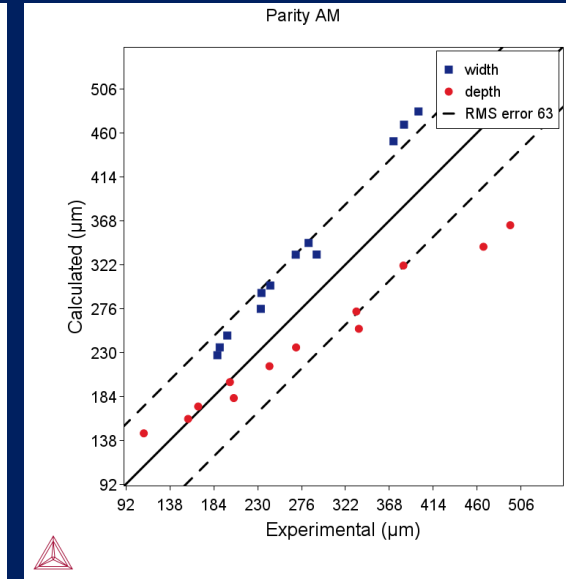
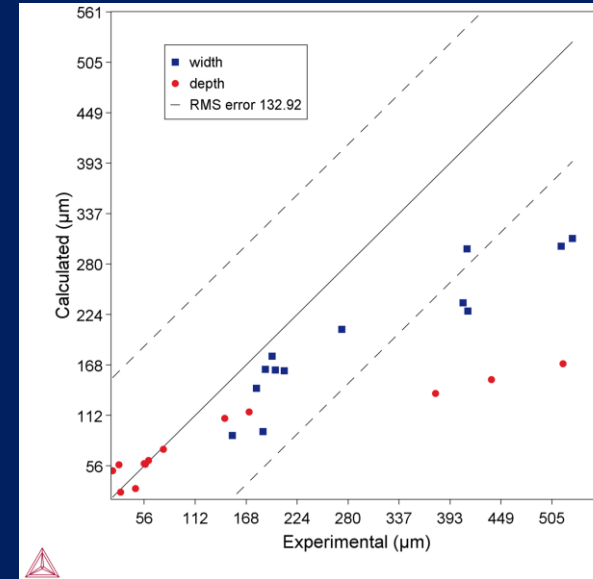
Experimental alloy:

- Absorptivity v/s temperature for Ni-, Fe-, Ti-, Al-based alloys
- Can then be calculated from Scheil for most alloys (alloy agnostic approach)
- But what about oxides (powder reuse, environment)?

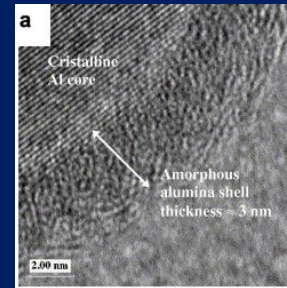
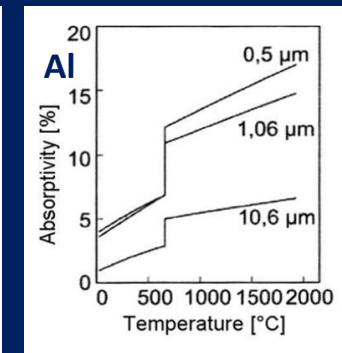
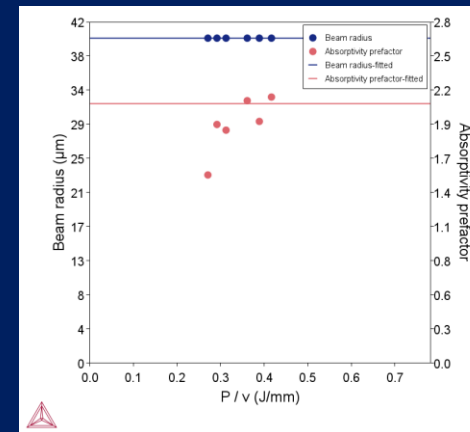
Experimental setup:

Beam size/absorptivity is not known.

Experimental information on process parameters and resulting melt pool dimensions are known.



Before/after adjusting absorptivity pre-factor for AlSi10Mg

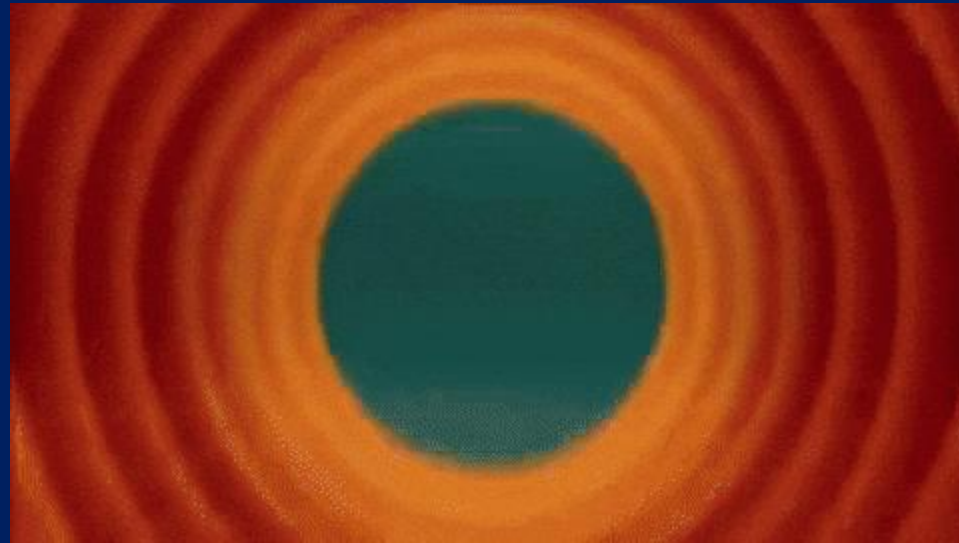


Al<sub>2</sub>O<sub>3</sub> at surface of Al-powder [Rufino et al., 2007]

# Summary of course

- Generate temperature dependent properties for your alloy (alloy agnostic approach). Possible due to comprehensive databases providing thermophysical and thermodynamic properties
- FE solver can calculate temperature distribution and melt pool shape in a computationally efficient manner (as compared to FVM models)
- Such simulations provide microstructural information
  - Formation of defects upon printing (lack of fusion/ keyhole)
  - Primary grain morphology ( $G$  vs  $v$  plot)
  - Massive phase transformations (Martensite?)
- Information about AM simulation can be coupled to diffusion, precipitation and property models to know what happens inside the material upon printing
- Upcoming features: PBF-EB/ DED, Beam shaping, Ray tracing models and many more!

The end. Questions?



Write to us at [info@thermocalc.com](mailto:info@thermocalc.com) or [bharat@thermocalc.com](mailto:bharat@thermocalc.com)  
Please wait for providing feedback and let us know how this went